# Chapter 11

# Computational approaches for extremal geometric eigenvalue problems

# Chiu-Yen Kao<sup>a</sup>, Braxton Osting<sup>b</sup>, and Edouard Oudet<sup>c,\*</sup>

<sup>a</sup>Department of Mathematical Sciences, Claremont McKenna College, Claremont, CA, United States, <sup>b</sup>Department of Mathematics, University of Utah, Salt Lake City, UT, United States, <sup>c</sup>LJK, Université Grenoble Alpes, Saint-Martin-d'Hères, France

## **Contents**

1	Introduction					2.4.5	Numerical results	392
2	Maximizing Laplace-Beltrami eigenvalues on closed surfaces			379			g Steklov eigenvalues ct surfaces with boundary	393
	<ul><li>2.1 Maximizing Laplace–Beltrami eigenvalues on flat tori</li><li>2.2 Conformal Laplace–Beltrami eigenvalues</li></ul>		380	3.1		rmization of multiply ected domains	394	
			383	3.2	Comp	Computational methods		
		0	Numerical methods	384		3.2.1	Solving the Euclidean	
	2.3		Numerical experiments ogical Laplace–Beltrami	385			Steklov eigenproblem (20)	395
	eigenvalues			386		3.2.2	Optimization methods	
		2.3.1	Genus $\gamma = 0$ closed surfaces	386			for extremal Steklov eigenvalues (21)	396
		2.3.2	Genus $\gamma = 1$ closed surfaces	387		3.2.3	Parameterizing the geometry	396
	2.4		nizing Laplace–Beltrami values on embedded			3.2.4	Gradient based optimization methods	396
		surfac		388	2.2	O 1:	•	390
			Numerical methods Spectral method for	390	3.3		nality conditions and oundary minimal surfaces	397
			eigenpair computation	390		3.3.1	Computing the free	
		2.4.3	Representation of $\gamma$ and eigenvalue variations	391			boundary minimal surface from the	
		2.4.4	Optimization methods	392			Steklov eigenfunctions	398

<sup>\*</sup>Corresponding author: e-mail address: edouard.oudet@imag.fr

<sup>☆</sup> Chiu-Yen Kao acknowledges partial support from NSF grant DMS-1818948 and DMS-2208373. Braxton Osting acknowledges partial support from NSF DMS 17-52202. Édouard Oudet acknowledges partial support from CoMeDiC (ANR-15-CE40-0006) and ShapO (ANR-18-CE40-0013).

 $(k \ge 2)$ 

minimal surfaces 399
3.4.1 First nontrivial
eigenvalue (k = 1) 399
3.4.2 Higher eigenvalues

4 Disc	cussion and future directions	402
4.1	Future directions: spectral	
	geometry	402
4.2	Future directions:	
	computational methods	403
Ackno	wledgments	403
References		

## **Abstract**

In an extremal eigenvalue problem, one considers a family of eigenvalue problems, each with discrete spectra, and extremizes a chosen eigenvalue over the family. In this chapter, we consider eigenvalue problems defined on Riemannian manifolds and extremize over the metric structure. For example, we consider the problem of maximizing the principal Laplace–Beltrami eigenvalue over a family of closed surfaces of fixed volume. Computational approaches to such extremal geometric eigenvalue problems present new computational challenges and require novel numerical tools, such as the parameterization of conformal classes and the development of accurate and efficient methods to solve eigenvalue problems on domains with nontrivial genus and boundary. We highlight recent progress on computational approaches for extremal geometric eigenvalue problems, including (i) maximizing Laplace–Beltrami eigenvalues on closed surfaces and (ii) maximizing Steklov eigenvalues on surfaces with boundary.

402

## **Keywords**

Laplace operator, Dirichlet-to-Neumann operator, Steklov eigenvalue, Eigenvalue optimization, Free boundary minimal surface, Densest lattice sphere packing problem

## **MSC Codes**

35P05, 35P15, 49Q05, 58J50, 52C17, 65N25

## 1 Introduction

Extremal eigenvalue problems originate with Lord Rayleigh's fascinating conjecture that, of all two-dimensional Euclidean domains of fixed area, it is the disk that has the smallest principal Laplace–Dirichlet eigenvalue. Over the past 120 years, this conjecture was proven and an abundance of generalizations and related problems have been extensively studied (Henrot, 2006). Recently, there has been much interest in generalizing these ideas to more general geometric settings; we refer to such problems as *extremal geometric eigenvalue problems*. For example, rather than extremize the principal Laplacian eigenvalue over two-dimensional Euclidean domains, we might extremize the principal Laplace–Beltrami eigenvalue over a class of Riemannian manifolds of a fixed volume. In this setting, many analytic tools have recently been developed that, *e.g.*, describe the derivative of an eigenvalue with respect to a perturbation of the

metric (Berger, 1973; Bando and Urakawa, 1983; Soufi and Ilias, 2008) or describe the resulting spectrum when two manifolds are "glued" together at a point (Nadirashvili and Penskoi, 2018; Karpukhin et al., 2021; Karpukhin, 2021). Consequently, there are now several extremal geometric eigenvalue problems for which the optimal manifold is known (Hersch, 1970; Nadirashvili, 1996, 2002; Petrides, 2014; Nadirashvili and Sire, 2017; Karpukhin et al., 2021); such optimizers typically have very "nice" structure, e.g., the ball, the round sphere, kissing balls, kissing round spheres, the equilateral flat torus, etc.

However, for extremal geometric eigenvalue problems where the optimal manifold doesn't have such structure, we have hope that numerical optimization methods can be used to compute optimal manifolds and complement analytic tools to gain insight into the optimal structure. Such numerical methods build on the foundation of methods for extremal eigenvalue problems on Euclidean domains; see, e.g., Oudet (2004); Osting (2010); Antunes and Freitas (2012); Osting and Kao (2013, 2014); Antunes and Oudet (2017); Bogosel et al. (2017); Akhmetgaliyev et al. (2017). However, these more general geometric problems present new computational challenges and require novel numerical tools, such as the parameterization of conformal classes and the development of accurate and efficient methods to solve eigenvalue problems on manifolds with nontrivial genus and boundary. In this chapter, we review recent progress on computational approaches for extremal geometric eigenvalue problems. In particular, we focus on two problems:

- §2 maximizing Laplace–Beltrami eigenvalues on closed surfaces;
- §3 maximizing Steklov eigenvalues on compact surfaces with boundary.

For each of problem, we describe how the geometric structure is parameterized, the methods for computing eigenvalues, and the optimization methods used to solve the extremal eigenvalue problem. We consider several variations of these problems where the class of admissible surfaces consists of flat surfaces only, surfaces where the metric is constrained to a particular conformal class, and closed surfaces which can be embedded in three-dimensional Euclidean space. Our aim in this chapter is to provide a glimpse of the possibilities of using computational methods for extremal geometric eigenvalue problems and, as such, we have indicated in §4 several open problems and future directions.

## Maximizing Laplace-Beltrami eigenvalues on closed surfaces

Let (M,g) be a connected, compact Riemannian surface and  $\Delta_{M,g}$  $|g|^{-\frac{1}{2}}\partial_i|g|^{\frac{1}{2}}g^{ij}\partial_i$  denote the Laplace–Beltrami operator. The Laplace–Beltrami eigenproblem is to find eigenvalues  $\lambda = \lambda(M, g)$  and eigenfunctions,  $\psi =$  $\psi(x) = \psi(x; M, g)$ , satisfying

$$-\Delta_{M,g} \psi(x) = \lambda \psi(x), \qquad x \in M.$$
 (1)

The spectrum is discrete and we enumerate the eigenvalues, counting multiplicity, in the increasing order:  $\lambda_0(M,g) < \lambda_1(M,g) \le \lambda_2(M,g) \le \cdots \to \infty$ (Chavel, 1984). We will consider the problem of maximizing the k-th Laplace— Beltrami eigenvalue over a class of closed surfaces with a fixed volume constraint. This is equivalent to maximizing the "normalized" eigenvalue

$$\bar{\lambda}_k(M, g) := \lambda_k(M, g) \cdot \text{vol}(M, g),$$

which is computationally advantageous as it avoids an explicit volume constraint.

To describe the class of surfaces, (M, g), over which we'll maximize  $\lambda_k(M,g)$ , it is useful to recall a few definitions and results. Given a metric  $g_0$ , we say that a metric g is *conformal* to  $g_0$  if there exists a positive smooth function  $\omega \colon M \to \mathbb{R}_+$  such that  $g = \omega g_0$ . The conformal class,  $[g_0]$ , consists of all metrics conformal to  $g_0$ . By the uniformization theorem, every closed Riemann surface of genus  $\gamma = 0$  is conformal to the Riemann sphere, i.e., there is only one conformal class for genus  $\gamma = 0$  surfaces. A generalization of the uniformization theorem states that every closed genus  $\gamma = 1$  Riemann surface

is conformal to an (a, b)-flat torus generated by the basis matrix  $B = \begin{pmatrix} 1 & a \\ 0 & b \end{pmatrix}$ 

where  $(a,b) \in F := \{(a,b) \in \mathbb{R}^2 : a \in \left(-\frac{1}{2}, \frac{1}{2}\right], b > 0, a^2 + b^2 \ge 1\}$ . Thus, the genus  $\gamma = 1$  conformal classes are parameterized by  $(a, b) \in F$ . With these uniformization results in mind, for a given surface  $(M, g_0)$ , we could consider perturbations to the metric only within the conformal class  $[g_0]$  or also include perturbations that are nonconformal. This decomposition defines several optimization problems depending on what type of perturbation is allowed. In section 2.1, we consider the problem where we restrict the class of surfaces to flat tori; the metric only varies over the conformal classes (i.e.,  $(a, b) \in F$ ) and not within each conformal class. Actually, here, we consider this problem not just in two dimensions, but in higher dimensions as well and show that the optimization problem for the k = 1 eigenvalue is equivalent to finding the densest lattice sphere packing. In section 2.2, we consider the problem where the metric only varies within a fixed conformal class,  $[g_0]$ . In section 2.3, we consider the combined problem where the metric is allowed to vary over all smooth metrics on the surface. Finally, in section 2.4 we consider a different kind of constraint where only embedded closed surfaces are considered.

#### Maximizing Laplace-Beltrami eigenvalues on flat tori 2.1

Consider the d-dimensional lattice  $\Gamma_B := B\mathbb{Z}^d$  generated by the basis matrix  $B \in GL(d,\mathbb{R})$  and the *d*-dimensional flat torus  $T_B := \mathbb{R}^d / \Gamma_B$ . The volume of  $T_B$  is given by  $\operatorname{vol}(T_B) = |\det B|$ . Each eigenpair,  $(\lambda, \psi)$ , of the Laplacian,  $-\Delta$ , on  $T_B$  corresponds to an element of the dual lattice,  $\Gamma_B^* = B^{-t} \mathbb{Z}^d = \Gamma_{B^{-t}}$ :

$$\lambda = 4\pi^2 \|w\|^2, \qquad \psi(x) = e^{2\pi i \langle x, w \rangle}, \qquad \forall w \in \Gamma_R^*.$$

The multiplicity of each nonzero eigenvalue is even since  $w \in \Gamma_B^*$  and -w correspond to the same eigenvalue. It follows that the eigenvalues of  $-\Delta$  on  $T_B$ ,

$$0 = \lambda_0 < \lambda_1 = \lambda_2 \le \lambda_3 = \lambda_4 \le \cdots$$

are characterized by the Courant-Fischer formulae,

enumerated in increasing order,

$$\lambda_k(T_B) = \min_{E \in \mathbb{Z}_{k+1}^d} \max_{v \in E} 4\pi^2 \|B^{-t}v\|^2, \tag{2}$$

where  $\mathbb{Z}_k^d := \{E \subset \mathbb{Z}^d : |E| = k\}$ . For  $k \in \mathbb{N}$ , define the *volume-normalized Laplacian eigenvalue*,  $\bar{\lambda}_k : GL(d, \mathbb{R}) \to \mathbb{R}$ , by

$$\bar{\lambda}_{k,d}(B) = \lambda_k(T_B) \cdot \text{vol}(T_B)^{\frac{2}{d}}.$$
 (3)

The volume-normalized eigenvalues are scale invariant in the sense that  $\bar{\lambda}_{k,d}(\alpha B) = \bar{\lambda}_{k,d}(B)$  for all  $\alpha \in \mathbb{R} \setminus \{0\}$ .

Here, for fixed  $k, d \in \mathbb{N}$ , we consider the extremal eigenvalue problem

$$\Lambda_{k,d} = \max_{B \in GL(d,\mathbb{R})} \bar{\lambda}_{k,d}(B). \tag{4}$$

A proof that there exists of a matrix  $B^*$  attaining the maximum in (4) can be found in Lagacé (2019, Theorem 1.1). Two tori,  $T_A$  and  $T_B$ , are isometric if and only if A and B are equivalent in  $O(d,\mathbb{R})\setminus GL(d,\mathbb{R})/GL(d,\mathbb{Z})$ . Here,  $O(d,\mathbb{R})$  is the group of orthogonal matrices and  $GL(d,\mathbb{Z})$  is the group of unimodular matrices. Since the Laplacian spectrum is preserved by isometry, it follows that the solution to the optimization problem in (4) is not unique. The uniqueness result up to isometry has been proved only for certain dimension d, e.g. 1, 2, 3, 8, and 24. It remains an open problem for other dimensions.

For general d and k, a maximizer for (4) is unknown. In dimension d=1, it is easy to see that  $\Lambda_{k,1}=4\pi^2\left\lceil\frac{k}{2}\right\rceil^2$ . In dimension d=2, it was shown by M.

Berger that 
$$\Lambda_{1,2} = \frac{8\pi^2}{\sqrt{3}}$$
 is attained by the basis  $B_{1,2}^{\star} = \begin{pmatrix} 1 & \frac{1}{2} \\ 0 & \frac{\sqrt{3}}{2} \end{pmatrix}$ , which gener-

ates the equilateral torus (Berger, 1973). It was shown in Kao et al. (2017) that for  $k \ge 1$ , there is a local maximum with value  $\Delta_{k,2} = 4\pi^2 \left\lceil \frac{k}{2} \right\rceil^2 \left( \left\lceil \frac{k}{2} \right\rceil^2 - \frac{1}{4} \right)^{-\frac{1}{2}}$  and that this is the global maximum for k = 1, 2, 3, 4. For each k, the corresponding eigenvalue has multiplicity 6 and value is attained by a flat torus

generated by the lattice with basis 
$$B_{k,2}^{\star} = \begin{pmatrix} 1 & \frac{1}{2} \\ 0 & \left( \left\lceil \frac{k}{2} \right\rceil^2 - \frac{1}{4} \right)^{\frac{1}{2}} \end{pmatrix}$$
.

In higher dimensions, the following proposition shows that there is a relationship between the principal volume-normalized eigenvalue,  $\bar{\lambda}_{1,d}$ , and the

densest lattice sphere packing problem (Conway and Sloane, 1999). Recall that for a given lattice,  $\Gamma_A$ , the *density* of a sphere packing with centers at  $\Gamma_A$  is given by

 $\mathcal{P}$  = proportion of space that is occupied by the spheres.

The kissing number,  $\tau$ , associated with the sphere packing is the number of other spheres each sphere touches.

**Proposition 2.1.** Let  $B \in GL(d, \mathbb{R})$  and let  $\bar{\lambda}_{1,d}(B) = \lambda_1(T_B) \cdot \operatorname{vol}(T_B)^{\frac{2}{d}}$  be the corresponding principal volume-normalized eigenvalue of the flat torus  $T_B :=$  $\mathbb{R}^d/\Gamma_B$ . Let  $\mathcal{P}$  be the packing density for the arrangement of balls with centers on the dual lattice,  $\Gamma_B^* = B^{-t} \mathbb{Z}^d$ . Then

$$\bar{\lambda}_{1,d}(B) = 16\pi^2 \omega_d^{-\frac{2}{d}} \mathcal{P}^{\frac{2}{d}},$$
 (5)

where  $\omega_d$  denotes the volume of a d-dimensional ball. Furthermore, the kissing number,  $\tau$ , of the packing is the multiplicity of  $\lambda_1(T_B)$ .

*Proof.* Using the Courant–Fischer formulae (2) with k = 1,  $\lambda_1(T_B) =$  $\min_{E \in \mathbb{Z}^d \setminus \{0\}} 4\pi^2 \|B^{-t}v\|^2$ , we see that  $\sqrt{\frac{\lambda_1}{4\pi^2}}$  is the length of the shortest vector in the lattice  $\Gamma_B^*$ . The density of a packing of balls with centers on the dual lattice,  $\Gamma_B^*$  is

$$\mathcal{P} = \frac{\text{volume of ball}}{\text{volume of fundamental region}} = \frac{\omega_d \rho^d}{|\det B^{-t}|} = \omega_d \rho^d |\det B|,$$

where  $\rho$  is the radius of the balls. Observing that the shortest vector in the lattice is exactly twice the radius of the ball packing, we have  $\sqrt{\frac{\lambda_1}{4\pi^2}} = 2\rho$ , giving  $\rho^2 = \frac{\lambda_1}{16\pi^2}$ . It then follows that  $\mathcal{P}^{\frac{2}{d}} = \omega_d^{\frac{2}{d}} \rho^2 (\det B)^{\frac{2}{d}} = \omega_d^{\frac{2}{d}} \frac{\lambda_1}{16\pi^2} (\det B)^{\frac{2}{d}} =$  $\omega_d^{\frac{2}{d}} \frac{1}{16\pi^2} \bar{\lambda}_{1,d}$ , as desired. 

Proposition 2.1 shows that maximizing the principal volume-normalized Laplacian eigenvalue of a d-dimensional torus  $T_B$  in (4) is equivalent to finding the lattice  $\Gamma_R^*$  that gives the densest packing of balls in d-dimensions. In this sense, the extremal eigenvalue problem on flat tori is *dual* to the densest lattice packing problem. Much is known about the densest lattice packings for small dimensions, d (Conway and Sloane, 1999). In particular, this problem is NP-hard and the values for the densest known lattices for dimension  $d = 1, \dots, 16, 24$ and corresponding volume-normalized Laplacian eigenvalues are tabulated in Table 1. For larger k, maximizing  $\bar{\lambda}_{k,d}$  is equivalent to the NP-hard problem of finding the d-dimensional (dual) lattice with longest k-th shortest lattice vector. The relationship between these two problems is further discussed in Kao et al.

**TABLE 1** For dimensions d = 1, ..., 16, 24, we tabulate the lattice with the largest known density  $\Gamma_R^*$ , the corresponding kissing number au, the density  $\mathcal{P}$ , and the volume-normalized eigenvalue of the torus,  $\Lambda_{1,d}(B)$ . All values except  $\Lambda_{1,d}$  appear in Conway and Sloane (1999, Table 1.2), for which we refer the reader to for details about the lattices.

d	$\Gamma_B^*$	τ	$\mathcal{P}$	$\Lambda_{1,d}(B)$
1	$A_1$	2	1	$4\pi^2 \approx 39.4784$
2	$A_2$	6	$\frac{\pi}{2\sqrt{3}} \approx 0.9069$	$\frac{8\pi^2}{\sqrt{3}} \approx 45.5858$
3	$D_3$	12	$\frac{\pi}{3\sqrt{2}} \approx 0.7405$	$4\pi^2 2^{\frac{1}{3}} \approx 49.7397$
4	$D_4$	24	$\frac{\pi^2}{16} \approx 0.6169$	$4\pi^2\sqrt{2}\approx 55.8309$
5	$D_5$	40	$\frac{4\pi^2}{15}2^{-\frac{5}{2}}\approx 0.4653$	$4\pi^2 2^{\frac{3}{5}} \approx 59.8381$
6	$E_6$	72	$\frac{\pi^3}{48\sqrt{3}} \approx 0.3729$	$8\pi^2 3^{-\frac{1}{6}} \approx 65.7460$
7	E <sub>7</sub>	126	$\frac{\pi^3}{105} \approx 0.2953$	$4\pi^2 2^{\frac{6}{7}} \approx 71.5131$
8	$E_8$	240	$\frac{\pi^4}{384} \approx 0.2537$	$8\pi^2 \approx 78.9568$
9	Λ9	272	$\frac{\sqrt{2}\pi^4}{945} \approx 0.1457$	$8\pi^2 \approx 78.9568$
10	$\Lambda_{10}$	336	$\frac{\pi^5}{2^7 15\sqrt{3}} \approx 0.0920$	$2^{\frac{1}{5}}3^{-\frac{1}{10}}8\pi^2 \approx 81.2613$
11	K <sub>11</sub>	432	$\frac{2^5 \pi^5}{3^5 385 \sqrt{3}} \approx 0.06043$	$2^{\frac{9}{11}}3^{-\frac{5}{11}}8\pi^2 \approx 84.4916$
12	K <sub>12</sub>	756	$\frac{\pi^6}{19440} \approx 0.0495$	$\frac{16\pi^2}{\sqrt{3}} \approx 91.1715$
13	K <sub>13</sub>	918	$\frac{2^6 3^{-\frac{5}{2}} \pi^6}{135135} \approx 0.02921$	$2^{-\frac{2}{13}}3^{-\frac{5}{13}}16\pi^2 \approx 93.0249$
14	$\Lambda_{14}$	1422	$\frac{\pi^7}{2^4 \cdot 7! \sqrt{3}} \approx 0.02162$	$2^{\frac{3}{7}}3^{-\frac{1}{14}}8\pi^2 \approx 98.2477$
15	$\Lambda_{15}$	2340	$\frac{2^4 \pi^7}{2027025\sqrt{2}} \approx 0.01686$	$2^{\frac{2}{5}}8\pi^2 \approx 104.1842$
16	Λ <sub>16</sub>	4320	$\frac{\pi^8}{16.8!} \approx 0.0147$	$8\sqrt{2}\pi^2\approx 111.6618$
24	Λ <sub>24</sub>	196,560	$\frac{\pi^{12}}{479,001,600} \approx 0.0019$	$16\pi^2 \approx 157.9137$

(2021). It is proved that the optimal tori degenerate as  $k \to \infty$  for dimension  $2 \le d \le 10$  (Lagacé, 2019). Numerical results in Kao et al. (2021) suggest that this is true for any dimension d.

#### 2.2 Conformal Laplace-Beltrami eigenvalues

For a fixed Riemannian surface  $(M, g_0)$  and integer k, the k-th conformal Laplace-Beltrami eigenvalue of  $(M, [g_0])$ , denoted  $\Lambda_k^c(M, [g_0])$ , is the supremum of the volume-normalized k-th eigenvalue over all metrics of the form  $\omega g_0$ ,

where  $\omega > 0$  is a smooth function on M, i.e.,

$$\Lambda_{k}^{c}(M, [g_{0}]) := \sup\{\bar{\lambda}_{k}(M, g) \colon g \in [g_{0}]\}$$
$$= \sup\{\bar{\lambda}_{k}(M, \omega g_{0}) \colon \omega \in C^{\infty}(M), \ \omega > 0\}$$
(6)

where  $\bar{\lambda}_k(M,g) := \lambda_k(M,g) \cdot \text{vol}(M,g)$ . For a surface  $(M,\omega g_0)$ , the Laplace– Beltrami eigenvalue problem (1) simplifies to

$$-\Delta_{g_0}\psi = \lambda\omega\psi. \tag{7}$$

The following proposition gives the variation of  $\lambda(M, \omega g_0)$  and  $\Lambda(M, \omega g_0)$  with respect to  $\omega$ ; a proof can be found in Kao et al. (2017).

**Proposition 2.2.** If  $(\lambda, \psi)$  be a simple eigenpair satisfying (7), then the variations of the eigenvalue,  $\lambda$ , and volume-normalized eigenvalue,  $\bar{\lambda}$ , with respect to a perturbation of the conformal function  $\omega$  are given by

$$\frac{d}{d\varepsilon}\bigg|_{\varepsilon=0} \lambda(\omega + \varepsilon \tilde{\omega}) = -\lambda \int_{M} \left(\frac{1}{\int_{M} u^{2} \omega d\mu_{g_{0}}} u^{2}\right) \tilde{\omega} d\mu_{g_{0}}$$
 (8a)

$$\frac{d}{d\varepsilon}\bigg|_{\varepsilon=0}\bar{\lambda}(\omega+\varepsilon\tilde{\omega}) = -\lambda \int_{M} \left(\frac{\int_{M} \omega d\mu_{g_{0}}}{\int_{M} u^{2}\omega d\mu_{g_{0}}}u^{2} - 1\right)\tilde{\omega}d\mu_{g_{0}}$$
(8b)

To make this problem numerically tractable, for constants  $0 < \omega_{-} < \omega_{+}$ , we solve the modified problem

$$\Lambda_k(M, [g_0], \omega_-, \omega_+) 
:= \max\{\bar{\lambda}_k(M, \omega g_0) : \omega \in L^{\infty}(M), \ \omega_- \le \omega(x) \le \omega_+, \ x \in M\}.$$
(9)

This extremum eigenvalue problem in (6) is similar to Krein's problem for nonhomogeneous membranes (Henrot, 2006, Ch. 9), except that here we have a closed surface (no boundary conditions). A convergence result for this approximation is proven in Kao et al. (2017, Prop. 1.1).

#### 2.2.1 Numerical methods

For a fixed surface  $(M, \omega g_0)$ , to solve the eigenproblem in (7), we use linear finite elements. To represent the density  $\omega$ , we first compute the first N eigenfunctions,  $\{\psi_i^0\}_{i\in[N]}$ , for  $(M,g_0)$  and take  $\omega$  as the linear combination  $\omega(x) = \sum_{i \in [N]} c_i \dot{\psi}_i(x), x \in M$ . To solve the optimization problem (9), we use the BFGS quasi-Newton method to determine a direction of ascent, and the stepsize is determined by an Armijo-Wolfe line search. A log-barrier interior-point method is used to enforce  $L^{\infty}(M)$  constraints. Further details are given in Kao et al. (2017).

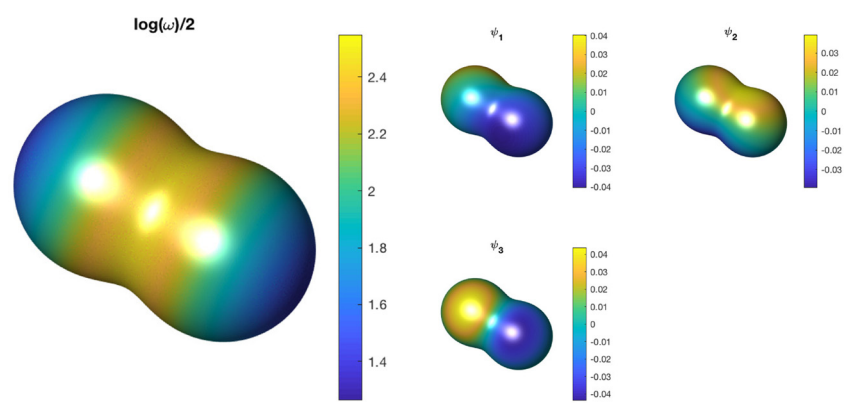


**FIGURE 1** (left) The best conformal factors found for maximizing  $\bar{\lambda}_1$  on a surface obtained by rotating the hippopede  $4x^2 + y^2 = (x^2 + y^2)^2$  around x-axis. (**right**) Eigenfunctions taken from the corresponding three-dimensional eigenspace.

## 2.2.2 Numerical experiments

We first consider the genus  $\gamma=0$  surface obtained by rotating the hippopede  $4x^2+y^2=(x^2+y^2)^2$  around x-axis, endowed with the embedded metric. It is known that the first conformal eigenvalue for this genus  $\gamma=0$  surface is  $8\pi^2$  (Hersch, 1970). The surface is represented by a triangular mesh with 104, 670 vertices and 209, 336 triangles. The maximum conformal factor found for the first eigenvalue (k=1) is plotted in Fig. 1(left) and attains the value  $\Lambda_1^c=8\pi\cdot0.999$ . This eigenvalue has multiplicity 3 and a basis for the eigenspace is plotted in the right panel of Fig. 1.

We now consider a genus  $\gamma=1$  surface given implicitly by  $\{(x,y,z)\in\mathbb{R}^3: (\sqrt{x^2+y^2}-1)^2+z^2=r^2\}$  where  $r\in(0,1)$  is fixed. It is known that this kind of torus is conformally equivalent to the (a,b)-flat torus with a=0 and  $b=\frac{r}{\sqrt{1-r^2}}$ ; see, e.g., Guenther et al. (2020). We consider the values  $r=\frac{2}{\sqrt{5}}$  and  $r=\frac{1}{\sqrt{2}}$ , for which we have b=2 and b=1, respectively. The tori are represented using triangular meshes with 32,014 vertices and 64,028 triangles for  $r=\frac{2}{\sqrt{5}}$  and 25,504 vertices and 51,008 triangles for  $r=\frac{1}{\sqrt{2}}$ . The maximum first eigenvalue is found to be  $\Lambda_1^c\approx30.99$  for  $r=\frac{2}{\sqrt{5}}$  and  $\Lambda_1^c\approx39.48$  for  $r=\frac{1}{\sqrt{2}}$ . For  $r=\frac{1}{\sqrt{2}}$ , it is known that the first conformal eigenvalue of the square flat torus is  $4\pi^2\approx39.48$  (El Soufi et al., 1996). For both  $r=\frac{2}{\sqrt{5}}$  and  $r=\frac{1}{\sqrt{2}}$ , the optimal conformal factors are invariant in the toroidal direction and the first eigenvalue has multiplicity 4. In Fig. 2, we plot the maximum conformal factor found for  $r=\frac{1}{\sqrt{2}}$  and a basis for the four-dimensional eigenspace.

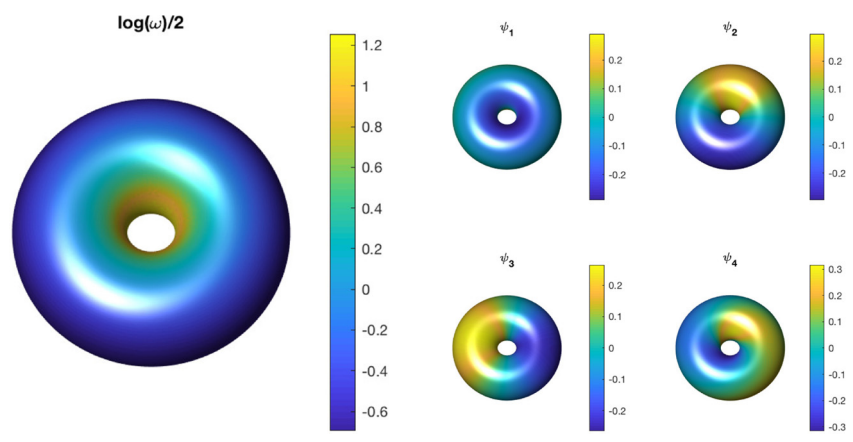


**FIGURE 2** (left) The best conformal factors found for maximizing  $\bar{\lambda}_1$  on a torus with  $r = \frac{1}{\sqrt{2}}$ . (right) Eigenfunctions taken from the corresponding four-dimensional eigenspace.

#### Topological Laplace-Beltrami eigenvalues 2.3

Let M be a (any) smooth closed manifold with genus  $\gamma$ . Let G(M) denote the class of Riemannian metrics g on M. For k fixed, the k-th topological Laplace— Beltrami eigenvalue for genus  $\gamma$  is defined

$$\Lambda_k^t(\gamma) := \sup\{\bar{\lambda}_k(M, g) \colon g \in G(M)\}. \tag{10}$$

# Genus $\gamma = 0$ closed surfaces

From the genus  $\gamma = 0$  uniformization theorem, we have  $\Lambda_k^t(0) = \bar{\lambda}_k^c(\mathbb{S}^2, g)$ .

For k = 1, it was shown by J. Hersch (Hersch, 1970) for k = 1 that  $\Lambda_1^t(0) \le$  $8\pi$  and equality is only attained by the round metric (up to isometry) on  $\mathbb{S}^2$ . This is equivalent to the first problem that we numerically solved in section 2.2.2.

For higher values of k, we can solve the problem numerically using the approach described in section 2.2 for conformal eigenvalues. Let us first discuss the case when k=2. Here, it is known that  $\Lambda_2^t(1)=16\pi\approx 50.26$  and is obtained by a sequence of surfaces degenerating to a union of two identical round spheres, i.e., two kissing spheres (Nadirashvili, 2002). Taking our base surface to be a sphere, represented using a triangular mesh with 40,962 vertices, we obtain a value of the numerical eigenvalue given by  $\Lambda_2 = 50.78$  which is slightly larger than the theoretical value. The conformal factor is displayed in Fig. 3(left) using the Hammer projection. We observe that the conformal factor has two localized regions with large values. To achieve better accuracy, we could locally refine the mesh at the regions. Alternatively, we consider surfaces that can resolve the singularity in the conformal factor. We consider surfaces in which two spheres have been "glued" together; see Fig. 3(center) and Fig. 3(right). When we solve the optimization problems on these meshes, the conformal factor is



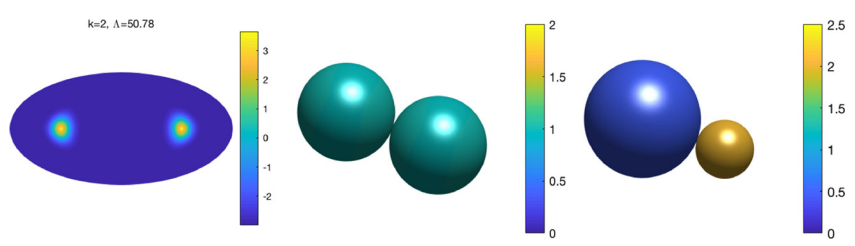


**FIGURE 3** The best conformal factors found for  $\Lambda_2^t$  on (**left**) the unit sphere with a Hammer projection view, (**center**) a genus zero mesh representing a union of two kissing unit spheres, and (**right**) on a genus zero mesh representing a union of a unit sphere and a sphere with radius 1/2.

smooth and approximately constant on each sphere. The obtained eigenvalues are  $\Lambda_2^t = 50.28$  and  $\Lambda_2^t = 50.26$ , respectively.

In Kao et al. (2017), this experiment was repeated for higher values of k and it was observed that on a sphere there were k localized regions where the conformal factor took large values and on k glued spheres, the conformal factor was smooth and approximately constant on each sphere. These computations supported the conjecture of N. Nadirashvili (2002) that  $\Lambda_k^t(0) = 8\pi k$ , attained by a sequence of surfaces degenerating to a union of k identical round spheres. This result was proven by M. Karpukhin, N. Nadirashvili, A. V. Penskoi, and Iosif Polterovich in 2021 (Karpukhin et al., 2021).

## 2.3.2 Genus $\gamma = 1$ closed surfaces

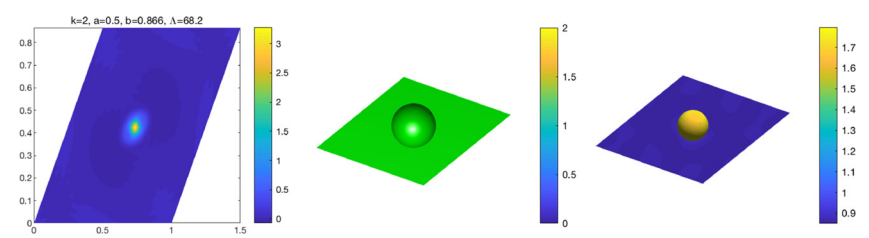
We now consider,  $\Lambda_k^t(1)$ , the k-th topological eigenvalue for genus  $\gamma=1$ . By the genus  $\gamma=1$  uniformization theorem, every Riemann surface is conformal to an (a,b)-flat torus for  $(a,b) \in F$ . In this case, to solve (10), we must allow the metric to vary over both the conformal classes and within each conformal class. For  $\gamma=1$ , the eigenproblem on the (a,b)-flat torus can be transformed via a (nonconformal!) linear map to the square domain,  $[0,2\pi]^2$ , giving the equation

$$-\Delta_{a,b} \psi = \omega \lambda(a,b,\omega) \psi \qquad \text{on } [0,2\pi]^2$$
 (11)

where 
$$\Delta_{a,b} = \frac{4\pi^2}{b^2} \left[ (a^2 + b^2) \partial_x^2 - 2a \partial_x \partial_y + \partial_y^2 \right]$$
 (Kao et al., 2017).

**Proposition 2.3.** (Kao et al., 2017, Prop. 4.2) Let  $\lambda(a,b,\omega)$  be a simple eigenvalue satisfying (11) for given  $(a,b) \in F$  and conformal factor  $\omega$ . Let the corresponding eigenfunction  $\psi$  be normalized such that  $\int_{[0,2\pi]^2} \psi^2(x,y) \omega(x,y) dxdy = 1$ . Then the derivative of  $\lambda$  with respect to the parameters a and b and the variation of  $\lambda$  with respect to a perturbation of the conformal function  $\omega$  are given by

$$\frac{\partial \lambda}{\partial a} = -\frac{b}{4\pi^2} \int_{[0,2\pi]^2} \psi(x,y) \Delta_a \psi(x,y) \, dx dy, \quad \Delta_a := \frac{4\pi^2}{b^2} \left[ 2a \partial_x^2 - 2\partial_x \partial_y \right]$$



(left) The best conformal factor and parameters (a, b) found on a meshed (a, b)- flat torus, (center) The best conformal factor found on a genus one mesh representing the union of a flat torus and a unit sphere. (right) The best conformal factor found on a genus one mesh representing the union of a flat torus and a sphere with radius a factor of 0.7 of the optimal radius.

$$\begin{split} \frac{\partial \lambda}{\partial b} &= -\frac{b}{4\pi^2} \int_{[0,2\pi]^2} \psi(x,y) \Delta_b \psi(x,y) \, dx dy, \quad \Delta_b := \frac{2\lambda \omega(x,y)}{b} + \frac{8\pi^2}{b} \partial_x^2 \\ \frac{d}{d\varepsilon} \bigg|_{\varepsilon=0} \lambda(\omega + \varepsilon \tilde{\omega}) &= -\lambda \frac{b}{4\pi^2} \int_{[0,2\pi]^2} \psi^2(x,y) \tilde{\omega}(x,y) \, dx dy. \end{split}$$

The derivatives of the volume-normalized eigenvalues can be obtained via the chain rule. We used the numerical methods described in section 2.2.1 to solve find the first few topological eigenvalue for genus  $\gamma = 1$ . The best result for k = 2 was  $\Lambda_2 \approx 68.20$  attained by an (a, b)-flat torus with (a, b) = $(0, 0.866) \approx (0, \frac{\sqrt{3}}{2})$  and a conformal factor that has one localized region with large values; see Fig. 4(left). To better resolve the singularity, we performed the calculation on a surface consisting of a flat torus glued to a sphere with the appropriate volume (Kao et al., 2017) and found that the best conformal factor converges to a constant function 1, as shown in Fig. 4(center). The obtained eigenvalue is  $\Lambda_2^t \approx 70.70$ , which is very close to  $\frac{8\pi^2}{\sqrt{3}} + 8\pi \approx 70.7185$ . In Fig. 4(right), the computation is repeated on a mesh representing a flat torus glued to a sphere with radius a factor of 0.7 of the optimal radius. The approach is able to identify the corresponding optimal conformal factor and the obtained eigenvalue is  $\Lambda_2^t \approx 70.70$ . In general, we conjecture that  $\Lambda_k^t(1) = \frac{8\pi^2}{\sqrt{3}} + 8\pi(k-1)$ , attained by a sequence of surfaces degenerating into a union of an equilateral flat torus and k-1 identical round spheres.

### 2.4 Maximizing Laplace-Beltrami eigenvalues on embedded surfaces

The Nash embedding theorem, named after John F. Nash, states that every Riemannian manifold can be isometrically embedded into some Euclidean space. It was already known to Gauss that there is no  $C^2$  isometric embedding of flat tori in Euclidean space, as at least two points of a  $C^2$  embedded surface have positive Gaussian curvature (the two points of contact with an osculating sphere). On the other hand, Nash and Kuiper showed that there exists a  $C^1$  isometric embedding

of the flat torus (Nash, 1954; Kuiper, 1955). Gromov introduced a convex integration theory that abstractly realized a sequence of embeddings which converge towards isometric embeddings (Gromov, 1970, 1986). Recently, V. Borrelli, S. Jabrane, F. Lazarus, and B. Thibert, further progressed these ideas by developing and implementing an algorithm that generates a sequence of increasingly "corrugated" surfaces degenerating into a fractal shape which is a  $C^1$  isometric embedding of the flat torus (Borrelli et al., 2012). The fourth iteration of this sequence was computed and the resulting figures and movies are striking.

In this section, we consider an alternative approach to finding an isometric embedding of the equilateral flat torus in Euclidean space. Our approach relies on the following theorem of N. Nadirashvili.

**Theorem 2.4** (Nadirashvili, 1996). Among all orientable, genus one surfaces of equal area, the equilateral flat torus attains the maximum first (nontrivial) Laplace–Beltrami eigenvalue,  $\Lambda_1 = \frac{8\pi^2}{\sqrt{3}} \approx 45.58$ .

An idea, suggested by A. Girouard, is then to start with a genus one embedded surface  $S_0 \subset \mathbb{R}^3$  and study the gradient flow of  $\bar{\lambda}_1(S) := \lambda_1(S) \cdot \text{vol}(S)$ . We reason that this flow, which we'll denote  $\{S_t : t \ge 0\}$ , should approach an embedded surface, isometric to the equilateral flat torus as  $t \to \infty$ . The surface flow cannot converge to a smooth surface, as this would violate the Nash embedding theorem. More generally, the conformal version of this problem can be posed where the conformal class of the embedded surfaces are constrained. A limitation of this approach, as compared to that of Borrelli et al. (2012), is that it only allows for the embedding of (a, b)-flat tori in conformal classes for which the flat metric is maximal, not all flat tori. Computational evidence suggests that this holds for (a, b)-flat tori with  $\{(a, b) \in F : a^2 + b^2 = 1\}$  (Kao et al., 2017). However, this alternative approach provides a new methodology to compute approximate isometric embeddings.

We will explore a direct parameterization method of embedded surfaces. This parametrization needs to be able to describe a sufficiently rich family of surfaces yet has Laplace-Beltrami eigenvalues which can be accurately and efficiently computed since an irregular behavior is expected. At some point during the flow, the surface may try to flow in a direction which would no longer be admissible e.g., the surface may attempt to "intersect itself" or increase its genus. Constraints should be enforced to prevent this from occurring. Furthermore, numerical implementation may encounter difficulty due to the potential nondifferentiability of  $\bar{\lambda}_1(S)$ . In fact, the first eigenvalue of the square flat torus has multiplicity 4 and the first eigenvalue of the equilateral flat torus has multiplicity 6. We describe in the following subsections our solutions to tackle these difficulties.

#### Numerical methods 2.4.1

We consider a family of surfaces of revolution,  $X: [0, 2\pi]^2 \to \mathbb{R}^3$ , given by

$$X(u, v) = \left(\gamma_1(u)\cos v, \ \gamma_1(u)\sin v, \ \gamma_2(u)\right) \tag{12}$$

which are generated by revolving the closed curve  $\gamma(u) = (\gamma_1(u), \gamma_2(u))$  with  $\gamma_1 > 0$  in the y-z plane around the z-axis. A straightforward calculation shows that the metric tensor g = g(u, v) is given by

$$g = \begin{bmatrix} X_u \cdot X_u & X_u \cdot X_v \\ X_u \cdot X_v & X_v \cdot X_v \end{bmatrix} = \begin{bmatrix} g_{11} & 0 \\ 0 & g_{22} \end{bmatrix}$$

where

$$g_{11}(u) = \gamma_1^2(u)$$
 and  $g_{22}(u) = \gamma_1'(u)^2 + \gamma_2'(u)^2$ .

Every surface in this parameterized family is conformally equivalent to a (0, b)flat torus where b depends on  $g_{11}$  and  $g_{22}$ . Thus,  $\Lambda_1$  is bounded above by  $4\pi^2 \approx$ 39.4784, which is attained by the flat metric on the square (0, 1)-torus (Kao et al., 2017).

The surface area of the embedded surface is given by  $A(\gamma)$  =  $2\pi \int_0^{2\pi} \sqrt{a(u)b(u)} du$  and the Laplace-Beltrami operator is

$$\Delta_g f = \frac{1}{a(u)} \partial_{vv} f + \frac{1}{\sqrt{a(u)b(u)}} \partial_u \sqrt{\frac{a(u)}{b(u)}} \partial_u f.$$

Separating variables and writing  $\Psi = U(u)V(v)$ , the eigenvalue equation  $-\Delta_g \Psi = \lambda \Psi$ , gives

$$-V''(v) = k^2 V(v), \quad \text{where } k \in \mathbb{N}$$
 (13a)

and

$$-\sqrt{\frac{a(u)}{b(u)}} \left( \sqrt{\frac{a(u)}{b(u)}} U'(u) \right)' + k^2 U(u) = \lambda a(u) U(u).$$
 (13b)

The solutions to (13b) give the eigenpairs  $(\lambda, \Psi)$  and, in particular, the normalized fundamental eigenvalue,

$$\bar{\lambda}_1(\gamma) = A(\gamma)\lambda_1(\gamma) = 2\pi\lambda_1(\gamma)\int_0^{2\pi} \sqrt{a(u)b(u)} \ du.$$

# Spectral method for eigenpair computation

To solve (13b) on  $[0, 2\pi]$  with periodic boundary conditions, we use a spectral method (Trefethen, 2000; Shen and Tang, 2006), which we briefly recall here.

A similar method was used in Kao et al. (2017). The discrete operator obtained by spectral collocation for the first derivative on a one-dimensional periodic grid on  $[0, 2\pi]$  with (odd) N points is represented by the Toeplitz matrix

$$D = \begin{pmatrix} 0 & -\frac{1}{2}\csc\frac{1h}{2} \\ -\frac{1}{2}\csc\frac{1h}{2} & \ddots & \ddots & +\frac{1}{2}\csc\frac{2h}{2} \\ +\frac{1}{2}\csc\frac{2h}{2} & \ddots & -\frac{1}{2}\csc\frac{3h}{2} \\ -\frac{1}{2}\csc\frac{3h}{2} & \ddots & \vdots \\ \vdots & \ddots & \ddots & +\frac{1}{2}\csc\frac{1h}{2} \\ +\frac{1}{2}\csc\frac{1h}{2} & 0 \end{pmatrix}$$

Here,  $h = \frac{2\pi}{N}$ . See, for example, Shen and Tang (2006, p. 83, Eq. 2.2.11a). We obtain a generalized eigenvalue problem

$$A\phi = \lambda B\phi,\tag{14}$$

which is solved using Matlab®'s built-in function eigs with default convergence criteria.

# Representation of $\gamma$ and eigenvalue variations

The closed curve  $\gamma: [0, 2\pi] \to \mathbb{R}^2$  is further parametrized using trigonometric functions,

$$\gamma_1(u) = 1 + \sum_{k=1}^{K} a_k \cos(ku) + b_k \sin(ku)$$
 (15a)

$$\gamma_2(u) = \sum_{k=1}^K c_k \cos(ku) + d_k \sin(ku). \tag{15b}$$

We require the variation of eigenvalues  $\lambda$  satisfying (14) with respect to the surface parameters,  $p = \{a_k, b_k, c_k, d_k\}_{k \in [K]}$  given in (15). In what follows we assume  $(\lambda, \phi)$  is a simple eigenpair satisfying (14). We consider a single parameter and denote the derivative with respect to this parameter using a dot. Taking derivatives of (14), we obtain

$$\dot{A}\phi + A\dot{\phi} = \dot{\lambda}B\phi + \lambda\dot{B}\phi + \lambda B\dot{\phi}.$$

Multiplying this equation on the left by  $\phi^t$ , using the symmetry of A and B, and assuming  $\phi$  is normalized by  $\phi^t B \phi = 1$ , we obtain the eigenvalue perturbation formula

$$\dot{\lambda} = \lambda \phi^t \dot{B} \phi - \phi^t \dot{A} \phi. \tag{16}$$

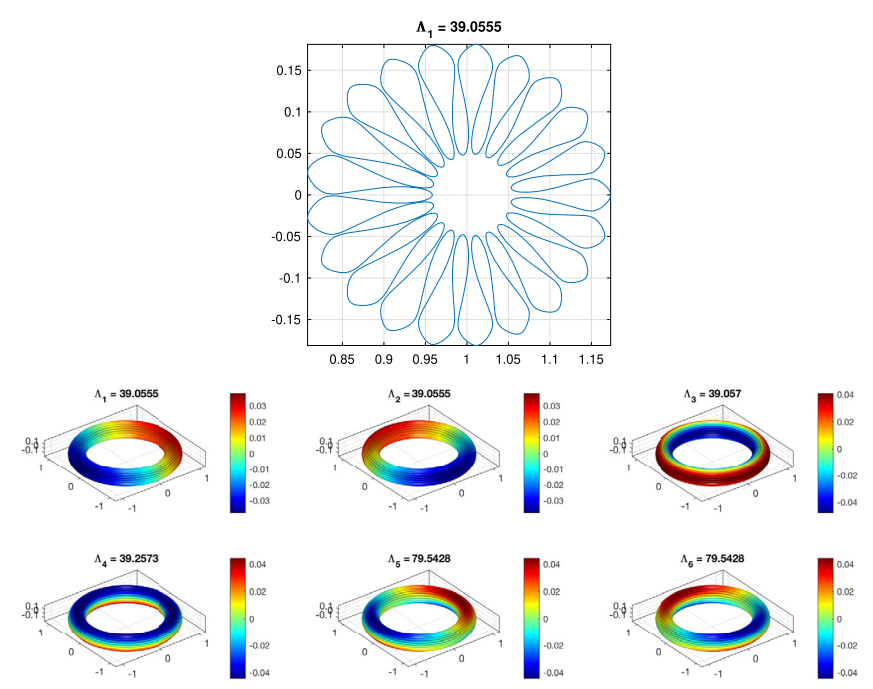


**FIGURE 5** The optimal surface found with  $\Lambda_1 = 39.0555$ . (top) The closed curve  $\gamma$  which generates the surface of revolution. (bottom) The first six eigenfunctions are plotted on the surface.

The matrices  $\dot{B}$  and  $\dot{A}$  can be computed analytically using the chain rule and the explicit dependence on the parameters in (15).

#### Optimization methods 2.4.4

To minimize  $p \mapsto \bar{\lambda}_1(S(p))$  for this choice of surface parameterization p, we use a gradient-based optimization method and the eigenvalue perturbation formula (16), In particular, we use the Broyden-Fletcher-Goldfarb-Shanno (BFGS) quasi-Newton method with an Armijo-Wolfe line search to adaptively choose the step size. To prevent self intersections during the optimization process, we sample N = 4K + 1 points on the closed curve  $\gamma$  and determine whether line segments connecting these points self-intersect after advancing the curve. If it does, a smaller step size is chosen to avoid self-intersections. This process has  $O(K^2)$  complexity.

#### 2.4.5 Numerical results

Summarizing, we consider surfaces of revolution X as in (12), where the closed curve  $\gamma$  is parameterized via (15) with a collection of parameters p = $\{a_k, b_k, c_k, d_k\}_{k \in [K]}$  with K = 64 coefficients. For such a surface, X = X(p), using the spectral collocation methods described above with N=257 discretization points, we can approximate  $p \mapsto \bar{\lambda}_1(p) = \bar{\lambda}_1(X(p))$ . We then use the BFGS quasi-Newton method to solve the optimization problem of maximizing  $\bar{\lambda}_1(p)$ , subject to the constraint that the surface does not self-intersect. As the surface evolves, we expect it to become increasingly oscillatory tending to an embedding of a square (0, 1)-flat torus. As shown in Fig. 5, the final curve  $\gamma = (\gamma_1, \gamma_2)$ on the y-z plane has a flower shape with 21 petals. For this surface, we have  $\Lambda_1 = 39.0555$  and multiplicity two. Also displayed in Fig. 5 are the first six Laplace–Beltrami eigenfunctions of the embedded surface. As one might expect from the ill-posedness of the problem, the computation is quite challenging and indeed the surface evolves irregularly. Nevertheless, the obtained results illustrate the idea and suggest that further numerical methods be employed to better prevent self-intersections and compute embedded surfaces with larger fundamental eigenvalue.

# Maximizing Steklov eigenvalues on compact surfaces with **boundary**

Let (M, g) be a smooth, compact, connected Riemannian surface with nonempty boundary,  $\partial M$ . The Steklov eigenproblem on (M, g) is given by

$$\Delta v = 0 \qquad \qquad \text{on } M \tag{17a}$$

$$\partial_{\nu}v = \sigma v$$
 on  $\partial M$ , (17b)

where  $\Delta$  is the Laplace–Beltrami operator and  $\partial_{\nu}$  is the outward normal derivative. The Steklov spectrum is discrete and we enumerate the eigenvalues, counting multiplicity, in increasing order:  $0 = \sigma_0(M, g) < \sigma_1(M, g) \le \sigma_2(M, g) \le$  $\cdots \to \infty$ . The Steklov spectrum coincides with the spectrum of the Dirichletto-Neumann operator  $\Gamma: H^{\frac{1}{2}}(\partial M) \to H^{-\frac{1}{2}}(\partial M)$ , given by the formula  $\Gamma w =$  $\partial_{\nu}(\mathcal{H}w)$ , where  $\mathcal{H}w$  denotes the unique harmonic extension of  $w \in H^{\frac{1}{2}}(\partial M)$  to M. The restriction of the Steklov eigenfunctions to the boundary,  $\{v_j|_{\partial M}\}_{j=0}^{\infty}$  $C^{\infty}(\partial M)$ , form a complete orthonormal basis of  $L^{2}(\partial M)$ . A recent survey on Steklov eigenvalues can be found in Girouard and Polterovich (2017).

We will consider the problem of maximizing the k-th Steklov eigenvalue over a class of compact surfaces with a boundary length constraint. To avoid the explicit constraint, we will again normalize the eigenvalue and consider the equivalent problem of maximizing

$$\bar{\sigma}_k(M,g) := \sigma_k(M,g) \cdot L(\partial M,g)$$

where  $L(\partial M, g)$  be the length of  $\partial M$  with respect to the metric g. For a fixed integer k and fixed manifold M with genus  $\gamma$  and b boundary components, we consider the extremal Steklov eigenvalue problem,

$$\Sigma_k(\gamma, b) := \sup_{g} \bar{\sigma}_k(M, g), \tag{18}$$

where g varies over the class of smooth Riemannian metrics on M.

Remark 3.1. As with Laplacian eigenvalues, the problem of maximizing over a fixed conformal class of metrics is of interest (Karpukhin and Métras, 2021); but here, we will consider the more general problem.

It is known that for any smooth Riemannian metric g, we have the following upper bound on the k-th Steklov eigenvalue

$$\Sigma_k(M, g) < 2\pi(\gamma + b + k - 1) \qquad \forall k \in \mathbb{N}. \tag{19}$$

This bound was proven by Weinstock (Weinstock, 1954) for k = 1,  $\gamma = 0$ , and b=1; by Fraser and Schoen (Fraser and Schoen, 2011) for k=1 (see also Girouard and Polterovich (2012)); and in generality by Karpukhin (Karpukhin, 2017). The existence of a smooth maximizer in (18) was established in Fraser and Schoen (2015, Theorem 1.1) for oriented surfaces of genus 0 with  $b \ge 2$ boundary components or a Möbius band and in Matthiesen and Petrides (2020) for general surfaces for the first (k = 1) eigenvalue.

Here, we review work that was published in Oudet et al. (2021) that develops computational methods for solving the extremal Steklov eigenvalue problem (18). It was shown in Fraser and Schoen (2013) that the optimality conditions for (18) generate a free boundary minimal surface in the ball. We review this optimal condition and use this approach to realize free boundary minimal surfaces beyond the known examples of equatorial disks, the critical catenoid, the critical Möbius band and their higher coverings.

#### 3.1 Uniformization of multiply connected domains

The conformal uniformization of multiply connected domains can be used to significantly reduce the complexity of the general Steklov eigenproblem (17) and extremal Steklov eigenproblem (18). The argument relies on two ingredients:

- 1. The uniformization result that for a compact, connected, genus-zero Riemannian surface with b boundary components,  $(\mathcal{M}, g)$ , there exists a conformal mapping  $f: (\mathcal{M}, g) \to (\Omega, \rho I)$ , where  $\Omega$  is a punctured disk with b-1holes and  $\rho I$  is a conformally flat metric.
- 2. The composition  $v \circ f$  of a function v with a conformal map f is harmonic if and only if v is harmonic.

Let  $D = \{x \in \mathbb{R}^2 \colon |x| \le 1\}$  be the unit disk and  $\Omega_{c,r} = D \setminus \bigcup_{i=1}^{b-1} D_i$  be a punctured unit disk with b-1 holes,  $D_i = D(c_i, r_i) = \{x \in \mathbb{R}^2 : |x - c_i| < r_i\},$  $i = 1, \dots, b-1$ . This argument implies that it is sufficient to consider the family of (flat!) Steklov eigenproblems,

$$\Delta u = 0 \qquad \qquad \Omega_{c,r} \tag{20a}$$

$$\partial_n u = \sigma \rho u \qquad \qquad \partial \Omega_{c.r}, \tag{20b}$$

where  $\Delta = \partial_x^2 + \partial_y^2$  is the Laplacian on  $\Omega$ ,  $\partial_n$  is the outward normal derivative, and  $\rho > 0$  is a density function. The extremal Steklov eigenvalue problem (18) for genus  $\gamma = 0$  is transformed to

$$\Sigma_k(\gamma = 0, b) = \max_{c_i, r_i, \rho} \Sigma_k$$
 (21a)

s.t. 
$$D_i \subset D$$
,  $i = 1, ..., b - 1$  (21b)

$$D_i \cap D_j = \varnothing, \qquad i \neq j$$
 (21c)

$$\rho(x) \ge 0, \qquad x \in \partial \Omega_{c,r}.$$
(21d)

Here,  $\Sigma_k = \sigma_k L$ ,  $\sigma_k$  is the k-th nontrivial eigenvalue satisfying (20), and L = $\int_{\partial\Omega_{c,r}} \rho(x) dx$  is the total length of  $\partial\Omega_{c,r}$ . The first two constraints simply state that the holes are contained in the domain and are pairwise disjoint.

#### 3.2 Computational methods

In section 3.1, we described how conformal maps could be used to reduce the general Steklov eigenproblem (17) to the Euclidean Steklov eigenproblem (20). In this subsection, we describe the computational methods used to solve the Euclidean Steklov eigenproblem (20) and optimization methods used to solve the extremal eigenvalue problem (18).

#### 3.2.1 Solving the Euclidean Steklov eigenproblem (20)

We require high precision in our solution to the Euclidean Steklov eigenproblem (20), since we want to use the approximate eigenfunctions satisfying the nonsmooth optimality conditions to generate a free boundary minimal surface. We use the method of particular solutions to solve the Steklov eigenproblem (20). This method for multiply-connected Laplace problems was recently discussed in Trefethen (2018). The methods rely on the following Theorem.

**Theorem 3.2** (Logarithmic Conjugation Theorem (Trefethen, 2018)). Suppose  $\Omega$  is a finitely connected region, with  $K_1, \ldots, K_N$  denoting the bounded components of the complement of  $\Omega$ . For each j, let  $a_i$  be a point in  $K_i$ . If u is a real valued harmonic function on  $\Omega$ , then there exist an analytic function f on  $\Omega$  and real numbers  $c_1, \ldots, c_N$  such that

$$u(z) = Re f(z) + c_1 \log|z - a_1| + \dots + c_N \log|z - a_N|, \qquad \forall z \in \Omega.$$

Let  $M \in \mathbb{N}^*$  and consider some fixed punctured disk  $\Omega_{c,r}$ . Based on Theorem 3.2, we define the finite basis  $\mathcal{B}$  to approximate solutions of eigenvalue problem (20) as the union of the harmonic rescaled real and imaginary parts of the functions

$$\mathcal{B} = \bigcup_{j=0}^{M} \left\{ z \mapsto z^{j} \right\} \bigcup_{i=1}^{k-1} \bigcup_{j=1}^{M} \left\{ z \mapsto \frac{1}{(z - c_{i})^{j}} \right\} \bigcup_{i=1}^{k-1} \left\{ z \mapsto \log|z - c_{i}| \right\}.$$

For instance, we rescaled the basis polynomial  $Re\left(\frac{1}{(z-c_2)^3}\right)$  by a factor  $r_2^3$  so that this basis function takes values of order 1 on the second circle. Consider now  $(p_l)_{1 \le l \le L}$  a uniform sampling with respect to arc length of  $\partial \Omega_{c,r}$ . Using  $\mathcal{B}$ , we approximate solutions of eigenvalue problem (20b) by the solution of the non symmetric square generalized eigenvalue problem

$$B^T A u_d = \sigma_d \ B^T B u_d$$
, where  $A = \left(\frac{\partial \phi}{\partial n}(p_l)\right)_{1 \le l \le L, \ \phi \in \mathcal{B}}$  and  $B = (\phi(p_l))_{1 \le l \le L, \ \phi \in \mathcal{B}}$ .

## Optimization methods for extremal Steklov eigenvalues (21)

We used gradient-based optimization methods to solve the extremal Steklov eigenvalue problem (21). We first describe our parameterization of the boundary.

#### 3.2.3 Parameterizing the geometry

Let  $\rho \in L^{\infty}(\partial \Omega_{c,r})$  be the boundary density and denote the restriction of  $\rho$  to the *i*-th disk boundary by  $\rho_i = \rho|_{\partial D(c_i,r_i)}$ ,  $i = 1, \dots, k-1$ . Thus, if  $\Omega_{c,r}$  has b boundary components, the geometry is described by the parameters

$$\{c_i\}_{i=1}^{b-1}, \qquad \{r_i\}_{i=1}^{b-1}, \quad \text{and} \quad \{\rho_i(x)\}_{i=1}^{b}.$$

Since  $\partial D(c_i, r_i) \cong \mathbb{S}^1$ , we expand each  $\rho_i$  in the truncated Fourier series

$$\rho_i(\theta) = A_{i,0} + \sum_{\ell=0}^{N} A_{i,\ell} \cos(\ell\theta) + B_{i,\ell} \sin(\ell\theta), \qquad \theta \in [0, 2\pi].$$

Due to the uniqueness of conformal mapping up to a Möbius transformation from a smooth, compact, genus-zero Riemann surface with b boundary components to a unit disk with b-1 circular holes (Gardiner and Lakic, 1999), it would be possible to center one of the holes at the origin and another on the positive x-axis. However, we found that the representation of the boundary density  $\rho$  for finite basis size (finite N) was better without fixing these centers.

# Gradient based optimization methods

As in Akhmetgaliyev et al. (2017), to handle multiple eigenvalues, we trivially transform (21) into the following problem

$$\max t$$
 (22a)

s.t. 
$$t \le \sigma_i L$$
  $i = k, k+1, \ldots$  (22b)

We approximated the positivity constraint  $\rho \geq 0$  by imposing the positivity on all L sample points,

$$\rho(p_{\ell}) \qquad \qquad \ell = 1, \dots, L. \tag{22c}$$

This approximation leads to linear inequalities with respect to the coefficients  $(A_{i,l}, B_{i,l})$  only. We also include the geometrical constraints in (21) by imposing the (few) quadratic constraints on the variables  $(c_i, r_i)_{1 \le i \le k-1}$ :

$$|c_i|^2 < (1 - r_i)^2$$
  $i = 1, \dots, k - 1,$  (22d)

$$|c_i - c_j|^2 > (r_i + r_j)^2$$
  $i, j = 1, ..., k - 1, j \neq i.$  (22e)

Using the derivatives computed in Oudet et al. (2021), together with the interior point method implemented in Byrd et al. (2006), we solved (22). All results of section 3.4, have been obtained with the following parameters: M = 30 (maximal order of basis elements),  $L = 10^4$  (number of sampling points) and at most 5000 iterations to reach a first order optimality condition criteria to a relative precision of  $10^{-6}$ . Observe that in all cases, we were able to recover the multiplicity three of the optimal eigenvalue up to 6 digits. In our implementation, the computational cost is proportional to the number of connected components of the boundary. For instance, one hour of computation on a standard laptop was required to obtain the desired precision for three boundary components.

#### Optimality conditions and free boundary minimal surfaces 3.3

Recently, A. Fraser and R. Schoen discovered a rather surprising connection between the extremal Steklov eigenvalue problem in (18) and the problem of generating free boundary minimal surfaces in the Euclidean ball (Fraser and Schoen, 2011, 2013, 2015). These findings have been further developed (Fan et al., 2014; Fraser and Schoen, 2019; Girouard and Lagacé, 2020) and were recently reviewed in Li (2019). Denote the closed n-dimensional Euclidean unit ball by  $\mathbb{B}^n := \{x \in \mathbb{R}^n : |x| \le 1\}$  and the (n-1)-dimensional unit sphere by  $\mathbb{S}^{n-1} = \partial \mathbb{B}^n$ . Let  $\mathcal{M} \subset \mathbb{B}^n$  be a d-dimensional submanifold with boundary  $\partial \mathcal{M} = \overline{\mathcal{M}} \cap \mathbb{S}^{n-1}$ . We say that  $\mathcal{M}$  is a free boundary minimal submanifold in the unit ball if

- (i)  $\mathcal{M}$  has zero mean curvature and
- (ii)  $\mathcal{M}$  meets  $\mathbb{S}^{n-1}$  orthogonally along  $\partial \mathcal{M}$ .

When d = 2, we call  $\mathcal{M}$  a free boundary minimal surface in the unit ball or, more simply, a free boundary minimal surface. For a good visual aid to understanding the definition of free boundary minimal surfaces, we recommend the reader take a look at the free boundary minimal surfaces displayed in Fig. 7.

Fraser and Schoen observed that a *d*-dimensional submanifold  $\mathcal{M} \subset \mathbb{B}^n$  with boundary  $\partial \mathcal{M} = \overline{\mathcal{M}} \cap \mathbb{S}^{n-1}$  is a free boundary minimal surface if and only if the coordinate functions  $x_i$ , i = 1, ..., n restricted to  $\mathcal{M}$  are Steklov eigenfunctions with eigenvalue  $\sigma = 1$ . Furthermore, they showed the following theorem.

**Theorem 3.3** (Fraser and Schoen, 2013). Let  $\mathcal{M}$  be a compact surface with boundary. Suppose that  $g_0$  is a smooth metric on  $\mathcal{M}$  attaining the supremum in (18) for some  $k \in \mathbb{N}$ . Let U be the n-dimensional eigenspace corresponding to  $\sigma_k(\mathcal{M}, g_0)$ . Then, there exist independent Steklov eigenfunctions  $u_1, \ldots, u_n \in U$  which give a (possibly branched) conformal immersion  $u = (u_1, \dots, u_n) \colon \mathcal{M} \to \mathbb{B}^n$  such that  $u(\mathcal{M})$  is a free boundary minimal surface in  $\mathbb{B}^n$  and, up to rescaling of the metric, u is an isometry on  $\partial \mathcal{M}$ .

Theorem 3.3 gives a method for using the solution of (18) to compute free boundary minimal surfaces. The simplest such example is the equatorial disk, obtained as the intersection of  $\mathbb{B}^3$  with any two-dimensional subspace of  $\mathbb{R}^3$ . This can be constructed from Weinstock's result that inequality in (19) with  $k = 1, \gamma = 0$ , and b = 1 is attained only by the round disk,  $\mathbb{D}$  (Weinstock, 1954). In this case, for the eigenvalue  $\Sigma_1(0,1) = 2\pi$ , we have the two-dimensional eigenspace given by span $\{x, y\}$ . The equatorial disk is given as the map  $u: \mathbb{D} \to \mathbb{D}$  $\mathbb{R}^2$ , defined by  $u(x, y) = \begin{pmatrix} x \\ y \end{pmatrix}$ .

For genus  $\gamma = 0$  and b = 2 boundary components, the extremal metric is rotationally invariant and the corresponding free boundary minimal surface is the critical catenoid. For genus  $\gamma = 0$  and  $b \ge 3$  boundary components, the extremal metric is not known explicitly, but it is known that the corresponding free boundary minimal surface is embedded in  $\mathbb{B}^3$  and star-shaped with respect to the origin (Fraser and Schoen, 2013). In Girouard and Lagacé (2020), the authors used homogenization methods to construct surfaces that have large first Steklov eigenvalue  $\bar{\sigma}_1$ . In particular, free boundary minimal surfaces of genus  $\gamma = 0$  with particular symmetries (e.g., symmetries of platonic solids) were constructed numerically. The authors proved that the first nonzero Steklov eigenvalue,  $\sigma_1$ , of these surfaces is 1 and emphasized that it is not known whether these surfaces have extremal first eigenvalues among all surfaces with the same genus and number of boundary components.

## Computing the free boundary minimal surface from the 3.3.1 Steklov eigenfunctions

At this point we assume that we have successfully solved the extremal Steklov problem (21) and want to use Theorem 3.3 to compute the associated free boundary minimal surface using the Steklov eigenfunctions. Let  $\sigma$  denote the optimal eigenvalue and assume that it has multiplicity n. Define the mapping  $v = [v_1, \dots, v_n]: \Omega \to \mathbb{R}^n$ , where  $\{v_i\}_{i=1}^n$  is some choice of basis for the ndimensional eigenspace. For  $A \in \mathbb{R}^n$ , we consider the map  $u_A : \Omega \to \mathbb{R}^n$ , defined by

$$u_A(x) = [v_1(x), \dots, v_n(x)] A, \qquad x \in \Omega.$$

We want to identify the matrix A so that the map  $u_A = u = [u_1, \dots, u_n]$  satisfies the spherical and the isothermal coordinate conditions,

$$|\partial_r u(r,\theta)|^2 = r^{-2} |\partial_\theta u(r,\theta)|^2, \qquad \forall (r,\theta) \in \Omega_{r,c}$$
 (23a)

$$\partial_r u(r,\theta) \cdot r^{-1} \partial_\theta u(r,\theta) = 0,$$
  $\forall (r,\theta) \in \Omega_{r,c}.$  (23b)

To this end, we construct the objective function

$$J(A) = \int_{\partial \Omega} W(u_A(x)) + \int_{\Omega} \left( |\partial_r u_A(r,\theta)|^2 - r^{-2} |\partial_\theta u_A(r,\theta)|^2 \right)^2 + |\partial_r u_A(r,\theta) \cdot r^{-1} \partial_\theta u_A(r,\theta)|^2,$$
(24)

where  $W(u) = \frac{1}{4}(|u|^2 - 1)^2$ . We then minimize J(A) over  $A \in \mathbb{R}^{n \times n}$ . Using this method, in all experiments in section 3.4, we were able to obtain three eigenfunctions which take values in the sphere on  $\partial \Omega$  to an absolute pointwise error bounded by  $10^{-3}$ . Moreover, since we have a parameterization of the surface, using the well-known analytic formula, we were able to compute the mean curvature of the surfaces, which in all cases was bounded by  $10^{-2}$ . The mean curvature and the Gaussian curvature are plotted on the free boundary minimal surface at Oudet (2020). Additionally, the angle that the boundary makes with the normal vector to the sphere is less than one degree.

## 3.4 Numerical solutions of the extremal Steklov eigenvalue problem and the corresponding free boundary minimal surfaces

In this section, we report numerical solutions for the extremal k-th Steklov eigenvalue problem with b boundary components and genus  $\gamma$ , along with the corresponding free boundary minimal surfaces (FBMS). For brevity, we only report results for selected values of b and k; the results of additional computations can be found in Oudet et al. (2021) on E. Oudet's website (Oudet, 2020), along with gifs.

# First nontrivial eigenvalue (k = 1)

For genus  $\gamma = 0$  and  $b = 2, \dots, 9, 12, 15, 20$  boundary components, we numerically solve the extremal Steklov problem (21) for the first nontrivial (k = 1) eigenvalue. The optimal values obtained are tabulated in Table 2. In each case, the multiplicity of the extremal eigenvalue is three, as expected (Fraser and Schoen, 2015).

Results of the computation for b = 3 are shown in Fig. 6. In Fig. 6(top), we plot the optimal punctured disk,  $\Omega_{c,r}$ , along with three linearly independent eigenfunctions corresponding to the eigenvalue  $\lambda_1 = 12.011987$ . Interestingly, the holes in the domain are slightly asymmetrically configured. The eigenfunctions plotted in do not exhibit symmetries, but this could be a result of our (arbitrary) choice within the three dimensional eigenspace. In Fig. 6(bottom),

**TABLE 2** For different numbers of boundary components b, we report the value of the first nontrivial normalized Steklov eigenvalue  $\Sigma_1 = \sigma_1 L$ , and the configuration of the centers of the boundary components.

b	$ar{\sigma}_1$	Boundary component configuration
2	10.4748	(critical catenoid) Digon
3	12.0120	equilateral triangle
4	13.6676	regular tetrahedron
5	14.4687	triangular bipyramid
6	15.4292	regular octahedron
7	15.9520	pentagonal bipyramid
8	16.4954	square antiprism (not regular)
9	16.9707	triaugmented triangular prism
12	18.0687	regular icosahedron
15	18.7934	triangular symmetry
20	19.7076	irregular, not dodecahedron

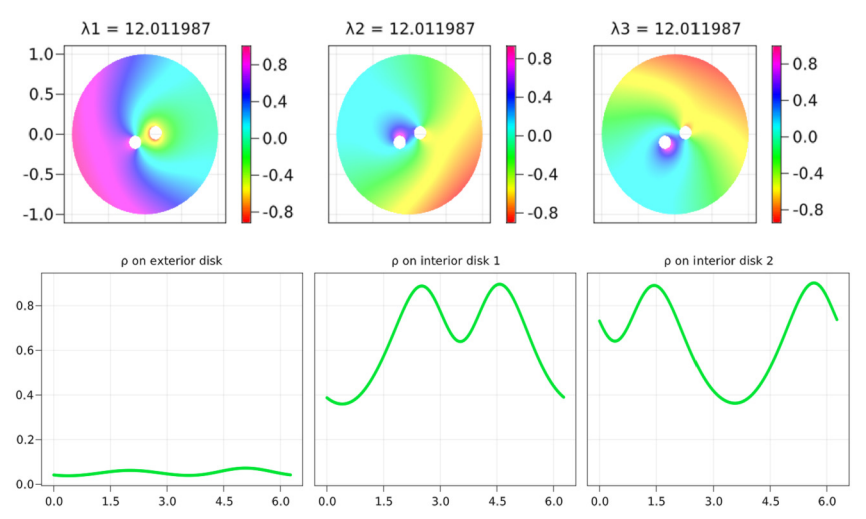


**FIGURE 6** (top) For b = 3 connected components of the boundary, we plot three linearly independent eigenfunctions associated to the first eigenvalue plotted in the domain with the optimal disk configuration. (bottom) Optimal densities on the three boundary components.

we plot the corresponding optimal densities on the exterior and two interior disks, which do not exhibit symmetry.

The free boundary minimal surfaces generated by maximizing the fundamental (k = 1) Steklov eigenvalue on genus  $\gamma = 0$  surfaces with b =2-6, 8, 9, 12, 15, 20 boundary components are plotted in Fig. 7. In all cases, the boundary components of the free boundary minimal surfaces are positioned at



**FIGURE** 7 Free boundary surfaces generated by maximizing the fundamental (k = 1) Steklov eigenvalue on  $\gamma = 0$  surfaces with b = 2-6, 8, 9, 12, 15, 20 boundary components as well as the k = 3 Steklov eigenvalue on  $\gamma = 0$  surfaces with b = 3, 4 boundary components.

very symmetric locations. The arrangement of the centers of the boundary components is described in Table 2. Interestingly, the free boundary minimal surface for b = 8 and b = 20 do not have the symmetry of the cube and regular dodecahedron, respectively. It seems that the positions of the boundary components are related to the minimizing configurations for Thompson's problem; known as the Fekete points (Fekete, 1923; Brown, 2020). We note that the free boundary minimal surfaces obtained here are closely related to the k-noid surfaces; see Weber (2020). It may be appropriate to the free boundary minimal surfaces computed here as *critical k-noids*. Further description of these free boundary minimal surfaces, as well as a comparison to the surfaces obtained in Girouard and Lagacé (2020) can be found in Oudet et al. (2021).

#### 3.4.2 Higher eigenvalues $(k \ge 2)$

Here, we consider the extremal Steklov eigenvalue problem (21), for higher eigenvalues,  $\Sigma_k$ ,  $k \ge 2$ . Less is known in this case and, in particular, the multiplicity of the optimal eigenvalue, and hence the dimension in which the free boundary minimal surface exists, is unknown. We recall the result of Fraser and Schoen (2019, Theorem 5.3), that the degenerate surface consisting of the critical catenoid glued to k-1 unit disks, is a free boundary minimal surface with b=2 boundary components in 3+2(k-1) dimensions with k-th normalized Steklov eigenvalue,  $\Sigma_k = \Sigma_1 + (k-1)2\pi$ .

We numerical solve the k = 3 Steklov problem (21) on  $\gamma = 0$  surfaces with b = 3,4 boundary components. The resulting free boundary minimal surfaces are displayed in Fig. 7. The eigenvalues obtained are  $\Sigma_3 = 23.6659$  (b = 3) and  $\Sigma_3 = 27.3103$  (b = 4). This b = 3 solution is only a local maximizer, because if we glue two disks to the surface attained by maximizing the first eigenvalue with b=3 boundary components, we obtain a b=3 free boundary minimal surface with third normalized Steklov eigenvalue  $\Sigma_3 = 12.0120 + 4 \cdot \pi \approx 24.5784$ .

## Discussion and future directions

In this chapter, we have demonstrated how computational approaches to such extremal geometric eigenvalue problems present new computational challenges and require novel numerical tools, such as the parameterization of conformal classes and the development of accurate and efficient methods to solve eigenvalue problems on domains with nontrivial genus and boundary. We have highlight recent progress on computational approaches for extremal geometric eigenvalue problems, including (i) maximizing Laplace-Beltrami eigenvalues on closed surfaces and (ii) maximizing Steklov eigenvalues on compact surfaces with boundary.

#### 4.1 Future directions: spectral geometry

In section 2.1, we discussed maximizing the principal Laplace–Beltrami eigenvalues on flat tori. For larger k, maximizing  $\lambda_{k,d}$  is equivalent to the NP-hard problem of finding the d-dimensional (dual) lattice with shortest k-th longest lattice vector. In Kao et al. (2021), the relationship between these two problems will be further investigated.

It is a very natural question to consider higher genus surfaces ( $\gamma \geq 2$ ). Here the surface is hyperbolic and the dimension of the space of conformal classes is known to be  $6(\gamma - 1) + 3b$ , where  $\gamma$  is the genus and b is the number of boundary components. There are parameterizations for this space, known as Fenchel-Nielsen coordinates. But the implementation of the glued "pairs of pants" is nontrivial. Furthermore, an efficient implementation would require derivatives with respect to the 'length' and 'twist' parameters (the analogue of Proposition 2.3), which we view as a challenging problem.

In section 2.4, we discussed how maximizing a Laplace-Beltrami eigenvalue on an embedded surface can be used to compute an isometric embedding of a flat torus. This extremal eigenvalue approach could be used to compute embeddings for other surfaces, such as the Bolza surface ( $\gamma = 2$ ).

#### Future directions: computational methods 4.2

Eigenvalue optimization problems are generally challenging as eigenvalues are not differentiable when they coalesce. While there are many methods for handling nonsmooth optimization and, in particular, extremal eigenvalue problems, some of the problems studied here could use further attention and a more careful comparison of numerical methods should be conducted. In particular, while these methods typically try to close a duality gap or converge in the objective value, we need methods for which the optimality condition is satisfied at the numerically computed optimal point. For example, if we use the extremal Steklov eigenvalue approach to compute free boundary minimal surfaces, can we bound the error in the mean curvature in terms of the optimization problem?

One recurring theme in spectral geometry that we hope we've illustrated here is that many of the supremum are obtained in a singular limit (kissing balls or irregular embeddings). We think it is a very interesting problem to develop more computational methods for studying such singular limits.

# Acknowledgments

We would like to acknowledge helpful discussions with A. Girouard, M. Karpukhin, J. Lagace, and I. Polterovich.

## References

Akhmetgaliyev, E., Kao, C.-Y., Osting, B., 2017. Computational methods for extremal Steklov problems. SIAM Journal on Control and Optimization 55, 1226-1240. https://doi.org/10.1137/ 16m1067263.

Antunes, P.R., Freitas, P., 2012. Numerical optimization of low eigenvalues of the Dirichlet and Neumann Laplacians. Journal of Optimization Theory and Applications 154, 235–257. https:// doi.org/10.1007/s10957-011-9983-3.

Antunes, P.R., Oudet, E., 2017. Numerical minimization of Dirichlet Laplacian eigenvalues of fourdimensional geometries. SIAM Journal on Scientific Computing 39, B508-B521. https://doi. org/10.1137/16m1083773.

- Bando, S., Urakawa, H., 1983. Generic properties of the eigenvalue of the Laplacian for compact Riemannian manifolds. Tohoku Mathematical Journal, Second Series 35, 155–172.
- Berger, M., 1973. Sur les premiéres valeurs propres des variétés Riemanniennes. Compositio Mathematica 26, 129-149.
- Bogosel, B., Bucur, D., Giacomini, A., 2017. Optimal shapes maximizing the Steklov eigenvalues. SIAM Journal on Mathematical Analysis 49, 1645–1680. https://doi.org/10.1137/16m1075260.
- Borrelli, V., Jabrane, S., Lazarus, F., Thibert, B., 2012. Flat tori in three-dimensional space and convex integration. Proceedings of the National Academy of Sciences 109, 7218–7223.
- Brown, K., 2020. Min-energy configurations of electrons on a sphere. http://mathpages.com/home/ kmath005/kmath005.htm.
- Byrd, R.H., Nocedal, J., Waltz, R.A., 2006. Knitro: an integrated package for nonlinear optimization. In: Large-Scale Nonlinear Optimization. Springer, pp. 35–59.
- Chavel, I., 1984. Eigenvalues in Riemannian Geometry. Academic Press.
- Conway, J.H., Sloane, N.J.A., 1999. Sphere Packings, Lattices and Groups. Springer, New York. https://doi.org/10.1007/978-1-4757-6568-7.
- El Soufi, A., Ilias, S., Ros, A., 1996. Sur la première valeur propre des tores. Séminaire de théorie spectrale et géométrie 15, 17-23.
- Fan, X.-Q., Tam, L.-F., Yu, C., 2014. Extremal problems for Steklov eigenvalues on annuli. Calculus of Variations and Partial Differential Equations 54, 1043–1059. https://doi.org/10.1007/s00526-
- Fekete, M., 1923. Über die verteilung der wurzeln bei gewissen algebraischen gleichungen mit ganzzahligen koeffizienten. Mathematische Zeitschrift 17, 228-249. https://doi.org/10.1007/ bf01504345.
- Fraser, A., Schoen, R., 2011. The first Steklov eigenvalue, conformal geometry, and minimal surfaces. Advances in Mathematics 226, 4011–4030. https://doi.org/10.1016/j.aim.2010.11.007.
- Fraser, A., Schoen, R., 2013. Minimal surfaces and eigenvalue problems. Contemporary Mathematics, 105-121. https://doi.org/10.1090/conm/599/11927.
- Fraser, A., Schoen, R., 2015. Sharp eigenvalue bounds and minimal surfaces in the ball. Inventiones Mathematicae 203, 823–890. https://doi.org/10.1007/s00222-015-0604-x.
- Fraser, A., Schoen, R., 2019. Some results on higher eigenvalue optimization. Preprint. arXiv:1910. 03547.
- Gardiner, F., Lakic, N., 1999. Quasiconformal Teichmüller Theory. American Mathematical Society. https://doi.org/10.1090/surv/076.
- Girouard, A., Lagacé, J., 2020. Large Steklov eigenvalues via homogenisation on manifolds. Preprint. arXiv:2004.04044.
- Girouard, A., Polterovich, I., 2012. Upper bounds for Steklov eigenvalues on surfaces. Electronic Research Announcements in Mathematical Sciences 19, 77-85. https://doi.org/10.3934/era. 2012.19.77.
- Girouard, A., Polterovich, I., 2017. Spectral geometry of the Steklov problem. Journal of Spectral Theory 7, 321–359. https://doi.org/10.4171/jst/164.
- Gromov, M., 1970. A topological technique for the construction of solutions of differential equations and inequalities. Proc. Int. Congress Math. 2, 221-225.
- Gromov, M., 1986. Partial Differential Relations. Springer.
- Guenther, N.-E., Massignan, P., Fetter, A.L., 2020. Superfluid vortex dynamics on a torus and other toroidal surfaces of revolution. Physical Review A 101, 053606.
- Henrot, A., 2006. Extremum Problems for Eigenvalues of Elliptic Operators. Birkhäuser Verlag. https://doi.org/10.1007/3-7643-7706-2.
- Hersch, J., 1970. Quatre propriétés isopérimétriques de membranes sphériques homogenes. C. R. Acad. Sci. Paris Sér. AB 270, A1645–A1648 (in French).
- Kao, C.-Y., Lai, R., Osting, B., 2017. Maximization of Laplace-Beltrami eigenvalues on closed Riemannian surfaces. ESAIM Control, Optimisation and Calculus of Variations 23, 685-720. https://doi.org/10.1051/cocv/2016008.

- Kao, C.-Y., Osting, B., Turner, J., 2021. Flat tori with large Laplacian eigenvalues in dimensions up to eight. arXiv preprint. arXiv:2202.08351.
- Karpukhin, M., 2017. Bounds between Laplace and Steklov eigenvalues on nonnegatively curved manifolds. Electronic Research Announcements in Mathematical Sciences 24, 100-109. https:// doi.org/10.3934/era.2017.24.011.
- Karpukhin, M., 2021. Index of minimal spheres and isoperimetric eigenvalue inequalities. Inventiones Mathematicae 223, 335-377.
- Karpukhin, M., Métras, A., 2021. Laplace and Steklov extremal metrics via *n*-harmonic maps. https://arxiv.org/abs/2103.15204.
- Karpukhin, M., Nadirashvili, N., Penskoi, A.V., Polterovich, I., 2021. An isoperimetric inequality for Laplace eigenvalues on the sphere. Journal of Differential Geometry 118, 313-333. https:// doi.org/10.4310/jdg/1622743142.
- Kuiper, N.H., 1955. On  $C^1$ -isometric imbeddings. Indagationes Mathematicae 58, 545–556.
- Lagacé, J., 2019. Eigenvalue optimisation on flat tori and lattice points in anisotropically expanding domains. Canadian Journal of Mathematics 72, 967-987. https://doi.org/10.4153/ s0008414x19000130.
- Li, M., 2019. Free boundary minimal surfaces in the unit ball: recent advances and open questions. Preprint. arXiv:1907.05053.
- Matthiesen, H., Petrides, R., 2020. Free boundary minimal surfaces of any topological type in euclidean balls via shape optimization. Preprint. arXiv:2005.06051.
- Nadirashvili, N., 1996. Berger's isoperimetric problem and minimal immersions of surfaces. Geometric and Functional Analysis 6, 877-897.
- Nadirashvili, N., 2002. Isoperimetric inequality for the second eigenvalue of a sphere. Journal of Differential Geometry 61, 335–340.
- Nadirashvili, N., Sire, Y., 2017. Isoperimetric inequality for the third eigenvalue of the Laplace-Beltrami operator on  $s^2$ . Journal of Differential Geometry 107, 561–571.
- Nadirashvili, N.S., Penskoi, A.V., 2018. An isoperimetric inequality for the second non-zero eigenvalue of the Laplacian on the projective plane. Geometric and Functional Analysis 28, 1368-1393.
- Nash, J., 1954. C<sup>1</sup> isometric imbeddings. Annals of Mathematics 60, 383–396.
- Osting, B., 2010. Optimization of spectral functions of Dirichlet-Laplacian eigenvalues. Journal of Computational Physics 229, 8578–8590. https://doi.org/10.1016/j.jcp.2010.07.040.
- Osting, B., Kao, C.-Y., 2013. Minimal convex combinations of sequential Laplace-Dirichlet eigenvalues. SIAM Journal on Scientific Computing 35, B731-B750. https://doi.org/10.1137/ 120881865.
- Osting, B., Kao, C.-Y., 2014. Minimal convex combinations of three sequential Laplace-Dirichlet eigenvalues. Applied Mathematics & Optimization 69, 123-139. https://doi.org/10.1007/ s00245-013-9219-z.
- Oudet, É., 2004. Numerical minimization of eigenmodes of a membrane with respect to the domain. ESAIM Control, Optimisation and Calculus of Variations 10, 315–330. https://doi.org/10.1051/ cocv:2004011.
- Oudet, E., 2020. Personal website. https://membres-ljk.imag.fr/Edouard.Oudet/research/ SteklovMin/index\_n.php.
- Oudet, É., Kao, C.-Y., Osting, B., 2021. Computation of free boundary minimal surfaces via extremal Steklov eigenvalue problems. ESAIM Control, Optimisation and Calculus of Variations 27, 34. https://doi.org/10.1051/cocv/2021033.
- Petrides, R., 2014. Maximization of the second conformal eigenvalue of spheres. Proceedings of the American Mathematical Society 142, 2385-2394.
- Shen, J., Tang, T., 2006. Spectral and High-Order Methods with Applications. Science Press.
- Soufi, A.E., Ilias, S., 2008. Laplacian eigenvalue functionals and metric deformations on compact manifolds. Journal of Geometry and Physics 58, 89-104.
- Trefethen, L.N., 2000. Spectral Methods in MATLAB, Vol. 10. SIAM.

- Trefethen, L.N., 2018. Series solution of Laplace problems. The ANZIAM Journal 60, 1–26. https://doi.org/10.1017/s1446181118000093.
- Weber, M., 2020. Bloomington's virtual minimal surface museum. https://minimal.sitehost.iu.edu/archive/Spheres/Noids/Jorge-Meeks/web/index.html.
- Weinstock, R., 1954. Inequalities for a classical eigenvalue problem. Indiana University Mathematics Journal 3, 745–753. https://doi.org/10.1512/iumj.1954.3.53036.